Chemical Engineering Journal 213 (2012) 163–174

Contents lists available at SciVerse ScienceDirect

Chemical Engineering Journal

journal homepage: www.elsevier.com/locate/cej

Preparation and performance of a novel composite as a reactive resin for copper retention

Reda R. Sheha *

Nuclear Chemistry Department, Hot Lab Center, Atomic Energy Authority, P.O. 13759, Cairo, Egypt

HIGHLIGHTS

- Nickel hexacyanoferrate loaded on nanoscale iron ferrite was synthesized.
- The nano-resins had homogeneous geometric shapes with 15–25 nm average size.
- Copper removal was attained through participation of different mechanisms.
- The background electrolyte played a significant role in the extent of sorption.
- Copper was retained through reversible process forming multi-linear formations.

GRAPHICAL ABSTRACT

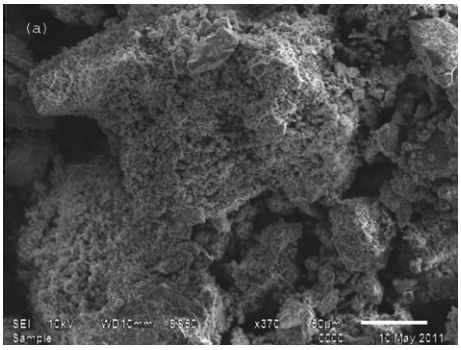

ARTICLE INFO

Article history:
Received 24 July 2012
Received in revised form 21 September 2012
Accepted 21 September 2012
Available online 11 October 2012

Keywords:
Magnetic nano-resins
Characterization
Cu(II) removal
Isotherm

ABSTRACT

A novel magnetic nano-resin was fabricated by supporting nickel hexacyanoferrate on Fe_3O_4 nanoparticles and immobilizing them within PAN matrix. The prepared composite was characterized using FTIR, TG–DTA, XRD, SEM and BET-N_2 measurements. The textural properties indicated the existence of slit-shaped pores and showed larger pores formed between plate-like particles. FTIR analysis suggested the presence of both hexacyanoferrate (II) and hexacyanoferrate (III) anions in the nano-composites. Further, data clarified a typical face-centered cubic structure with the molecular formula $K_2Ni[Fe(CN)_6]\cdot 3H_2O$. The resins were relatively fine, homogeneous with presence of little irregular clusters and had 15–25 nm average size. The kinetics of copper retention followed pseudo-second-order expression with k_2 values 3.81×10^{-5} g mg^{-1} min^{-1}. Copper sorption was pH-dependent and q_{max} was attained at pH 6.0 suggesting sorption by single Cu^{2+} species through molar exchange with either H^+ or K^+ ions at low pH values. In neutral solution, Cu^{2+} ions were retained by surface complexation besides ion exchange and hydrogen bonding interactions, while precipitation was the relevant mechanism taking place in basic medium. Intra-particle diffusion played a significant role at the initial stage of sorption and presence background electrolyte significantly reduced Cu^{2+} removal. Freundlich model appropriately described the removal of Cu(II) through a favorable sorption process.

1. Introduction

Heavy metals are chemical species extremely harmful for human beings, animals and plants. The improper disposal of these chemicals can cause serious environmental problems. Unlike organic pollutants, which are degradable species, metal ions do not easily get converted into harmless end products [1,2]. Heavy metals are continuously releasing from many industrial activities such as micro-electronics, electroplating, battery manufacture, metallurgical and fertilizer industries. Such activities feed water supplies with different heavy metals causing a serious environmental pollution in lakes, rivers, and groundwater [3–6].

* Tel.: +20 11 1589 4547.
E-mail addresses: reda.sheha@eaea.org.eg, rsheha68@yahoo.com

1385-8947/$ - see front matter © 2012 Elsevier B.V. All rights reserved.
http://dx.doi.org/10.1016/j.cej.2012.09.113

Copper is one of the major heavy metal contaminants that emanating environment from miscellaneous activities as electrical, electroplating and metal finishing industries. Often, it is found in high concentrations near mines, landfills and waste disposal sites. In human beings copper toxicity causes itching and dramatization, keratinization of hands and soles of feet [7]. Severe gastro-intestinal irritation and possible changes in liver and kidney occur due to intake of excessively large doses of copper. Further, inhalation of copper spray increases the risk of lung cancer among exposed workers [8,9]. Recent studies present evidence that copper plays a role in Alzheimer's disease [10].

Many processes have been developed to curtail heavy metal pollution, including chemical precipitation, electrolysis, reverse osmosis, solvent extraction, ion-exchange and sorption [11,12]. Among these methods, sorption technology has proven to be more viable alternative and increasingly receives more attention in recent years in removing heavy metal ions from wastewater [13]. For this purpose, extensive efforts were done to develop new materials could be used as sorbents for removal of such contaminants from waste solutions. Nowadays, many research efforts were devoted to apply nanoparticles in removal of different contaminants because of their unique properties and superior performance for potential applications in decontamination purposes [14]. This is because nanoparticles have extremely small size and high surface-area-to volume ratio provides better sorption kinetics. By rendering nanoparticles magnetic, through the acquisition of magnetism, a powerful new class of sorbent materials could be developed for fast and potential remediation purposes. These magnetic nanoparticles exhibit a finite-size effect resulting in a higher sorption capacity for metal removal as well as selective sorption properties and ease of phase separation [15,16].

Numerous types of magnetic nanoparticles could be tailored by supporting selective candidates on magnetic nanoparticles. In this concern, several studies reported a successful application of magnetic nano-structures in removal of different contaminants. Also, different transition metal hexacyanoferrates supported on Fe_3O_4 nanoparticles were effectively applied in treatments of radioactive wastes. Environmentally, Chitosan-based hydrogels with magnetite nanoparticles were effectively employed in adsorption of Pb(II), Cd(II), and Cu(II) ions from aqueous solutions [17], while Co(II) ions were successfully separated using magnetic chitosan nanoparticles [18]. Maor et al. [19] reported the removal of phosphate anions using granular activated carbon impregnated with nano-sized magnetite particles. In addition, magnetite polymeric resins were effectively used in remediation of water contaminated with Cr(VI) [20,21].

Studies addressing the removal of Cu(II) from waste solutions included the application of a wide variety of inorganic sorbents. One of these studies reported a fast adsorption of Cu(II) from aqueous solutions at pH 2–5 using carboxymethylated chitosan covalently bonded on Fe_3O_4 nanoparticles [22]. Further, Hizal and Apak [23] studied the uptake of Cu(II) using kaolinite clay minerals in presence of humic acid. The efficiency of Fe_3O_4 nanoparticles treated with Arabic gum to remove copper ions was also examined by Banerjee and Chen [10]. They suggested surface complexation as a possible mechanism in Cu(II) retention. Recently, meso-porous silica materials with silanol groups were effectively applied in Cu(II) removal [24]. Also, nano-aggregates of nickel hexacyanoferrate loaded magnetite were used for removal of cesium from radioactive wastes [25].

Although, the expected relevance of application of nickel imprinted hexacyanoferrates as sorbents, very little work was reported on usage of potassium nickel (II) hexacyanoferrate (II) supported on iron ferrite nanoparticles for retention of Cu(II). Therefore, the experimental work in this study was initiated on deposition of an insoluble hexacyanoferrate on magnetic nano-structured particles of Fe_3O_4 to produces an efficient nanocomposite could be utilized as a reactive resin for copper retention.

2. Experimental

2.1. Materials

All chemicals used were of analytical grade purity and used without further purification. A stock solution of 1000 mg L^{-1} Cu(II) ions was prepared by dissolving the required amount of $CuSO_4 \cdot 5H_2O$ in definite volume of bidistilled water and was used to prepare the desired concentrations of adsorbate solution by appropriate dilution. The Cu(II) solution, as prepared, had a pH value of 5.62 which did not change significantly with dilution. The pH value of aqueous solutions was stabilized by addition of 0.1 M HCl and/or NaOH solutions.

2.2. Preparation of Fe_3O_4 nanoparticles

Fe_3O_4 nanoparticles were prepared by co-precipitating Fe^{2+} and Fe^{3+} ions with ammonia solution in an inert atmosphere. Ferric and ferrous chlorides (molar ratio 2:1) were dissolved in bidistilled water at a concentration of 0.3 M iron ions. Chemical precipitation was achieved at 29 °C under vigorous stirring by adding NH_4OH solution (29.6%) and pH value was maintained at about 11 during precipitation process. Thereafter, the precipitate was dried at 60 °C for 60 min in presence of N_2 gas. The inert atmosphere prevents product oxidation according to the following equation:

$$2Fe_3O_4 + (1/2)O_2 \rightarrow 3Fe_2O_3 \quad (1)$$

The obtained nanoparticles were immersed in a solution of 10 mM HCl to induce positive surface charge, and then washed with bidistilled water until constant pH of 7.1 was sequentially attained. Positive charged species of Fe_3O_4 is needed for the precipitation of outer nickel hexacyanoferrate shell. Then, they were dried at room temperature and finally sieved to the desired mesh size.

2.3. Preparation of potassium nickel hexacyanoferrate

Metal ferrocyanides are usually prepared in a colloid form from soluble ferrocyanide, $K_4Fe(CN)_6$, and a divalent transition metal salt such as $NiCl_2$ by the following reaction:

$$Fe(CN)_{:6}^{4-} + 2M^{2+} + xH_2O \rightarrow M_2Fe(CN)_6 \cdot xH_2O \quad (2)$$

where M stands for a divalent element. Nickel hexacyanoferrate (NiHCNF) was prepared by adding 0.1 M $NiCl_2 \cdot 6H_2O$ solution gradually drop by drop into a 0.1 M $K_4Fe(CN)_6 \cdot 3H_2O$ solution under agitation. After complete addition of $NiCl_2$ solution, agitation was continued for more three hours. Then, the mixture was let to settle overnight, and supernatant was separated by decantation. After that, the precipitate was washed three times with bidistilled water and dried overnight under vacuum at room temperature.

2.4. Preparation of Fe_3O_4 @ NiHCNF nanoparticles

The magnetic Fe_3O_4 nanoparticles were used as a core in this preparation. For this purpose, a solution of 0.1 M $K_4Fe(CN)_6 \cdot 3H_2O$ was added to the positively charged Fe_3O_4 nanoparticles and agitated for 2 h in presence of N_2 gas. During this time, the positively charged Fe_3O_4 nanoparticles adsorb the negatively charged $Fe(CN)_{:6}^{4-}$; anion on their surface via electrostatic attraction. For the conversion of $K_4Fe(CN)_6$ adsorptively attracted to ferrite surface, a solution of 0.1 M $NiCl_2$ was slowly dropped into reaction mixture with vigorous stirring and in presence of N_2 gas. During this time, nickel hexacyanoferrate was precipitated as a thin layer on the surface of iron ferrite nanoparticles to produce a core–shell nano-structure. The mixture was further stirred for about 2 h, and let to settle down. The precipitate then was washed thoroughly

with bidistilled water until constant pH value was sequentially attained, and dried at room temperature in presence of N_2 gas (WM1). A part of the previously prepared composite was mixed with equivalent weights of polyacrylonitrile (PAN) in its gelatinous form. The obtained mixture was mixed well for homogeneous distribution of the solid particles along the binder matrix and kept in an oven at 50 °C overnight (WM2). Finally, the composites were pulverized, sieved to different mesh sizes. Particulates have mesh size range 0.170–0.135 mm were used in the rest of experiments.

2.5. Instrumentation

The surface characteristics of synthesized resins were characterized by Fourier Transform Infrared (FTIR) spectrophotometer Nicolet iS10, Thermo, USA. The powder X-ray diffraction patterns was recoded with Philips X-ray diffractometer model PW1710 equipped with monochromatized Cu Kα radiation (λ = 0.154 nm, 40 kV and 25 mA) employing a scan rate of 0.02° s^{-1} in the range from 10° to 70°. The thermal stability was verified using simultaneous DTA–TG 50 system from Shimadzu, Japan. TGA measurements were performed up to a temperature of 800 °C, with a heating rate of 5 °C min^{-1} using -Al_2O_3 as reference. Samples morphology and composition was analyzed using Scanning Electron Microscope (SEM) model JSM-6510A from JEOL, Japan. The specific surface area was determined from N_2 adsorption isotherm by BET method using a Nova 3200, Version 6.08 High Speed Gas Sorption Analyzer. The concentration of copper was determined using atomic absorption spectrometer (AAS). Analysis was performed using Solaar-II M5 atomic absorption spectrometer from Thermo Fisher Scientific Inc., Cambridge, UK. The measurements were carried out using Air-C_2H_2 flame with a fuel flow rate 1.1 L min^{-1} and the absorbance reading was detected at a wavelength of 324 nm.

2.6. Sorption experiments

Batch experiments were performed by equilibrating 0.1 g of magnetic resins with 10 mL of 50 mg L^{-1} Cu(II) solution in sealed glass bottles. The samples were shaken at 28 ± 2 °C and aliquots were taken at appreciate time intervals as necessary, centrifuged and the concentrations of Cu(II) were determined by atomic absorption spectrophotometer. The effect of hydrogen ion concentration on the amount of copper sorbed was studied by equilibrating 0.1 g resin with a set of 10 mL Cu(II) solutions. The initial pH value of these solutions was adjusted to different values ranged from 1 to 11 using 0.1 M HCl and/or 0.1 M NaOH solutions. In clarifying its effect as a background electrolyte, different initial concentrations of NaCl have the range 1×10^{-2} to 5×10^{-1} M were added to a set of copper solutions and equilibrated with a definite weight of prepared resins. After equilibrium, the samples were centrifuged and aliquots were subjected to AAS measurements. Similar experiments were carried out by contacting a fixed amount of adsorbents with 10 mL of Cu(II) solutions have varying concentrations cover the range of 10–100 mg L^{-1} and agitated till equilibrium. Then, resins were separated and metal ion concentration was determined by AAS. The sorption % and adsorbed amount (q) were calculated using the following equations:

$$Sorption\ \% = \frac{C_o - C_e}{C_o} \times 100 \quad (3)$$

$$q = (C_o - C_e) \times \frac{V}{m} \quad (4)$$

where C_o and C_e are the initial and equilibrium concentration of Cu(II) in aqueous solution, V is the aqueous volume (mL) and m is the weight of resin (g). All experimental data were the average of two replications of each experiment and the reproducibility of experimental measurements were mostly within ±2.4%.

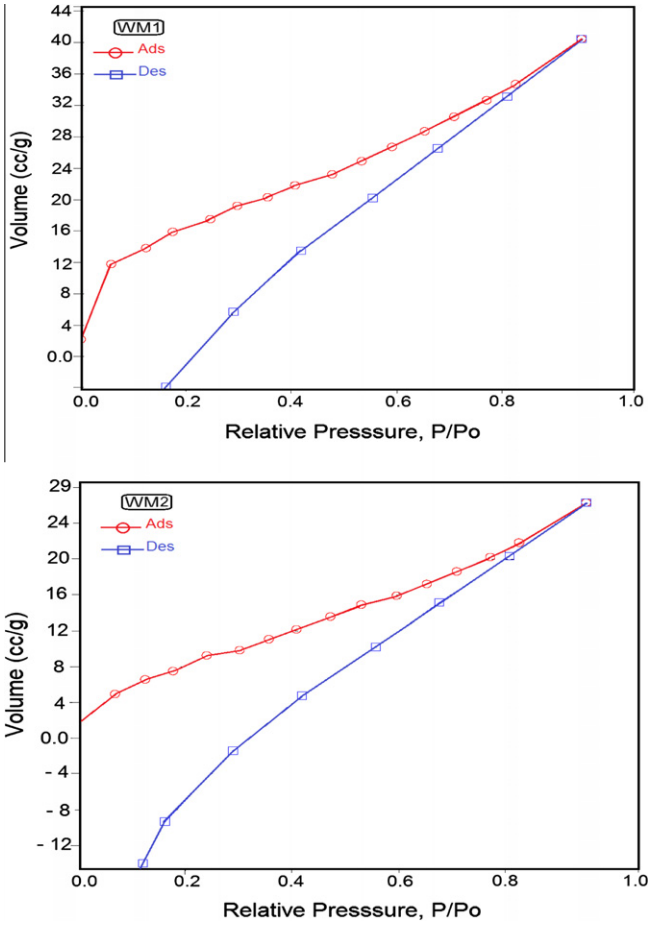

Fig. 1. The typical nitrogen adsorption–desorption isotherms for nickel hexacyanoferratemagnetic nano-resins.

3. Results and discussion

3.1. Characterization

The typical nitrogen adsorption–desorption isotherms for the synthesized nickel hexacyanoferrate magnetic resin (WM1) and the polymerized precursor (WM2) are shown in Fig. 1. The samples were firstly degassed before nitrogen adsorption measurement. The plots of nitrogen adsorption isotherm for both WM1 and WM2 samples, as they were prepared, could be classified as type-V with H3 hysteresis loop according to Brunauer–Deming–Deming–Teller (BDDT) classification. This classification indicated the existence of slit-shaped pores [26]. Also, the isotherms showed a hysteresis loop reflecting textural pores formed between plate-like particles [27]. The pore size distribution curves are quite broad and multimodal with small and large meso-pores. The small meso-pores reflect porosity in nano-flakes, while large ones could be related to the pores formed between stacked nano-flakes. The textural properties of synthesized materials, such as specific surface area, pore volume and average pore diameter, are listed in Table 1. The listed data show that WM1 sample had specific surface area of 61.01 $m^2\ g^{-1}$ with corresponding total pore volume of 6.26×10^{-2} $cm^3\ g^{-1}$, while WM2 resin had specific surface area of 33.76 $m^2\ g^{-1}$ with corresponding total pore volume of 4.07×10^{-2} $cm^3\ g^{-1}$.

FTIR spectra of magnetic resin (WM1) and the polymerized analogue (WM2) are recorded in Fig. 2. In both cases, the broad

Table 1
Textural properties of nickel hexacyanoferrate magnetic nano-resins.

Sample	S_{BET} ($m^2\ g^{-1}$)	D_p (nm)	V_t ($cm^3\ g^{-1}$)
WM1	61.01	2.05	6.26×10^{-2}
WM2	33.76	2.41	4.07×10^{-2}

S_{BET} is the specific surface area deduced from the isotherm analysis. D_p is the pore diameter calculated from the desorption branch of the isotherm. V_t is the total pore volume calculated at a relative pressure of 0.99.

absorption bands revealed at 3400 cm^{-1} was assigned to ν(OH) symmetric and asymmetric stretching of hydrogen bonded water molecules. The presence of coordinated water molecules existing in the interlayer structure was sensed around 1600 cm^{-1} due to δ(HOH) bending vibration. Also, this band could be ascribed to the stretching vibration of –N–H group. The characteristic peak for stretching vibration of C–H was observed at 2914 cm^{-1} and could be assigned to ν_a(C–H) [28]. Moreover, the band noted at 2240 cm^{-1} was implied to the vibration of –R–N group. These peaks are known as indicative bands of the function groups present in polyacrylonitrile structure that was used with sample WM2. The presence of these bands is an indicative to the successful coating of nano-particles with PAN [15]. The band detected at 1400 cm^{-1} might be attributed to the vibration interactions of surface –OH groups of Fe_3O_4 nanoparticles [29]. The bands arising around 2095 and 2045 cm^{-1} could be ascribed to ν(CN) stretching frequency of –CN groups in hexacyanoferrate (II). It was noteworthy that, hexacyanoferrate (II) ions are partly converted into hexacyanoferrate (III) ions during their aqueous interaction and vice versa [30]. The band sensed at 2045 cm^{-1} was due to hexacyanoferrate (II) ions while that observed at 2095 cm^{-1} was due to hexacyanoferrate (III) ions. The partial conversion of the hexacyanoferrate (II) ions to hexacyanoferrate (III) ions may be attributed to ligand exchange by water followed by oxidation interaction [31]. The split in ν(CN) stretching vibration is a common feature of potassium hexacyanoferrate salts [32]. Therefore, FTIR analysis suggests the presence of both hexacyanoferrate (II) and hexacyanoferrate (III) anions in both prepared samples. The bands revealed at 630 and 580 cm^{-1} could be assigned to the vibration of Fe–O. It is conceivable that the prepared resins are well coordinated and incorporated in the polymer matrix forming a more stable protecting layer.

The thermogravimetric analysis of the studied samples is given in Fig. 3. The figure shows the mass change and its derivative of nickel hexacyanoferrate magnetic resins heated with a rate of 5 °C min^{-1} up to 800 °C. It is clear that the dehydration process extended from 50 °C to ~300 °C was occurred in successive stages during which a reduction in sample mass by about 12.01% was detected. This value is close to the value 12.8% that represents the molecular mass of three water molecules relative to the molecular mass of nickel hexacyanoferrate molecule. In both resins, the thermal decomposition took place in three steps. The first mass loss was observer at a temperature range 50–120 °C and accompanied with an exothermic peak detected at 70.5 °C. This weight loss could be referred to removal of external water molecules. In second stage of dehydration process extended between 120 and 300 °C, the internal water molecules were escaped from crystal lattice of NiHCNF. In the range extended from 300 to 420 °C a loss in the weight of WM1 resin was observed and accompanied with an exothermic peak detected at 380.25 °C, Fig. 3a. This weight loss could be due to matrix decomposition with partial release of carbon, as CO_2, nitrogen, as NO_x and NH_3 leaving metal oxides of potassium, nickel and iron in the residue [31,33]. Fig. 3b shows that the decomposition of sample WM2 extended to 550 °C and was accompanied with an exothermic peak at 380.49 °C. Also, the decomposition of PAN organic binder took place causing a further weight loss in sample WM2 comparing with WM1. At higher temperature, no obvious weight loss was detected behind 550 °C for both samples.

It was obviously noted that TG curves of both resins are look similar while there was a slight difference in DTG curves. This slight difference was represented in the exothermic peak revealed at 339.28 °C which could be assigned to the decomposition of PAN organic binder used in preparation of WM2 resin. In the stage of dehydration extended between 50 and 300 °C, the detected weight loss represents the evolution of different two types of water molecules. One represents dehydration of external water molecules while the second denotes that escaped from crystal lattice. The dehydration process in such a manner is consistent with data revealed from FTIR investigation. FTIR spectra sensed the presence of two types of water molecules each of them has its peculiar character through ν(OH) and δ(HOH) vibrations.

The phase structure of prepared nickel hexacyanoferrate magnetic resin (WM1) as well as its PAN bonded precursors (WM2)

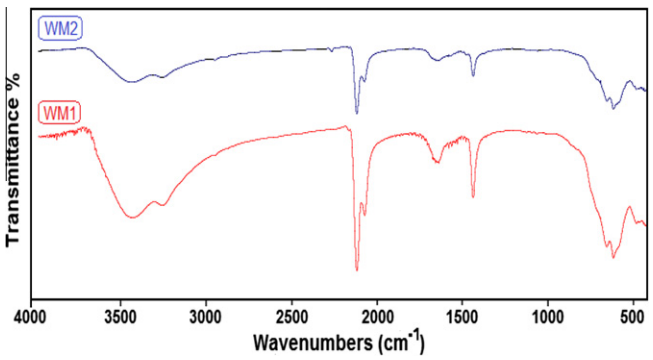

Fig. 2. FTIR spectra of prepared nickel hexacyanoferrate magnetic nano-resins.

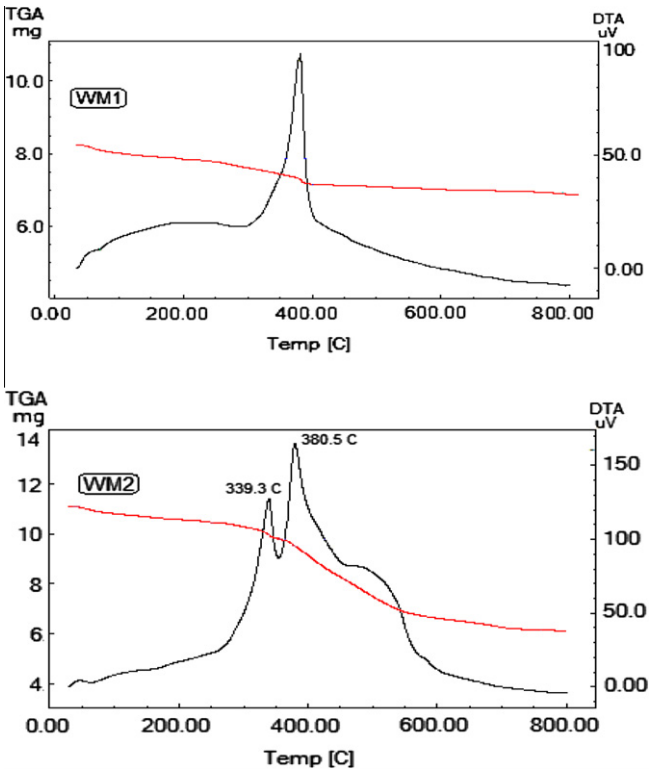

Fig. 3. Thermogravimetric analysis of prepared nickel hexacyanoferrate magnetic nano-resins.

was investigated by XRD and data are given in Fig. 4. The powder diffraction patterns of synthesized resins are similar to each other and matched well with that reported by Ambashta et al. [26]. The diffractograms indicated characteristic peaks at 2θ = 17.40°, 31.12°, 35.56°, 43.15°, 53.73°, 57.33°, and 64.86° related to the phases (001), (220), (311), (400), (422), (511) and (440), respectively. These X-ray patterns are consistent with the diffraction lines of both iron ferrite and potassium nickel hexacyanoferrate implying the presence of admixture of iron ferrite and nickel hexacyanoferrate. Further, the 00 l peak at 17.40° Confirmed the incorporation of hexacyanoferrate anions in the interlayer region of the iron oxide. All peaks were found to match well those of a typical face-centered cubic (FCC). The average crystallite size (L) was estimated using Debye–Scherrer equation [34]. The line broadening measurements were calculated from the half-width of the most intense peak of XRD patterns revealed at 2θ = 35.56° (line 311) that is common for potassium nickel hexacyanoferrate [35]. The calculated average crystallite size value was 10 and 11 nm for WM1 and WM2, respectively. Based on these data, a typical face-centered cubic structure with molecular formula $K_2Ni[Fe(CN)_6]\cdot 3H_2O$ was proposed for the prepared resins. This result coincides with that previously reported by other investigators [33,36].

The surface texture and morphology of nickel hexacyanoferrate magnetic resins are depicted in Fig. 5 and SM 1. It is evident from the scanning electro-micrographs (SEMs) that the particles of both synthesized resins are relatively similar and fine. They exhibited homogeneous structures had regular morphology with presence of little irregular clusters. The average size of most particles was in the range of 15–25 nm. Also, the nano-resins had wormhole like meso-porosity that most likely facilitates the analyte transport to access to the active sites during sorption processes, and finally improves the sorption efficiency. These features agree well with the textural properties that was depicted from N_2 adsorption–desorption isotherm. Additionally, WM2 sample was characterized with presence of a crust of PAN polymer coating its surface. At high magnification (x = 3500), SEM image further exhibited porous and ordered platelets separated from each other by many smaller particles forming a rugged layered network (Fig. 5b). The energy dispersive X-ray analysis (EDX) was performed for potassium nickel hexacyanoferrate and data are presented in Table 2. EDX elemental analysis supports the composition $K_{2.23}Ni_{1.08}[Fe_{1.35}(C_{6.03}N_{5.97})]$ as a formula supposed for the prepared resins. These results strongly support the previously proposed molecular formula of potassium nickel hexacyanoferrate.

3.2. Sorption kinetics

The kinetics of Cu(II) retention exhibited two sorption steps: a fast initial process followed by a much slower one. The sorption occurred rapidly at the early stage of reaction was probably due to the abundant availability of active sites on resins surface. With the gradual decrease in active sites, sorption was attained at a slower rate till reaching equilibrium. The prediction of sorption rate gives important information for selecting optimum operating conditions for full-scale batch process. In order to evaluate the kinetics that control the sorption process, simple first-order, pseudo-first-order and pseudo-second-order models were used to analyze the experimental data obtained from batch experiments.

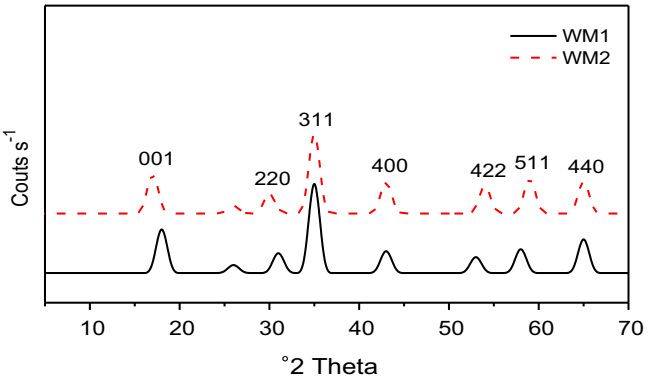

Fig. 4. XRD patterns of prepared nickel hexacyanoferrate magnetic nano-resins.

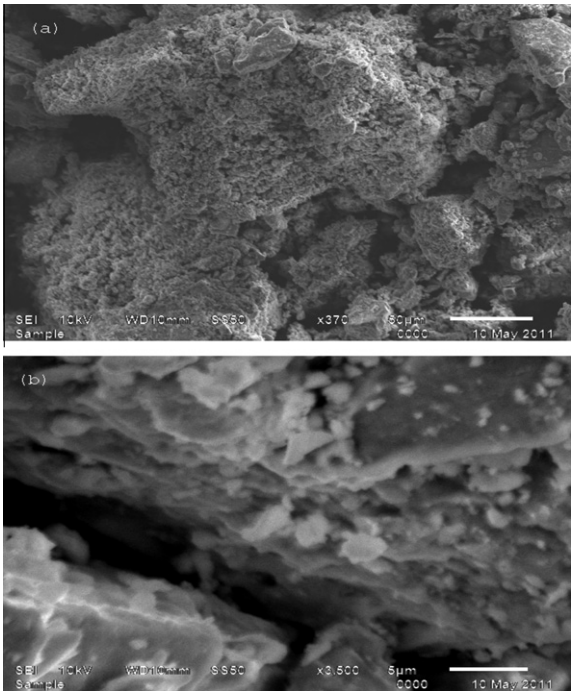

Fig. 5. SEM images of: (a) prepared nickel hexacyanoferrate magnetic nano-resin, (b) The corresponding magnified image.

Table 2
EDX analysis of nickel hexacyanoferrate resin.

Component	Weight (%)
C	36.15
N	35.84
K	13.37
Fe	8.15
Ni	6.49
Total	100.0

The sorption of copper ions from a liquid phase to a solid sorbent might be considered as a reversible reaction with an equilibrium state being established between two phases. Therefore, a simple first-order reaction model was used to correlate the rates of reaction, which could be expressed as [37]:

$$A \underset{k_b}{\overset{k_f}{\rightleftharpoons}} B \tag{5}$$

where k_f and k_b are the forward and backward reaction rate constants. If C is the initial concentration of copper and q is the amount transferred from liquid phase to nickel hexacyanoferrate magnetic nano-resin at any time t, then the rate will be:

$$\frac{\partial q}{\partial t} = -\frac{\partial}{\partial t}(c - q_t) = k(C - q_t) \tag{6}$$

where k is the overall reaction rate constant. Since k_f and k_b are the rate constants for the forward and reverse processes, then the rate equation can be expressed as:

$$\frac{\partial q}{\partial t} = k_f(C - q_t) - k_b q_t \quad (7)$$

If q_e represents the amount of copper sorbed on nickel hexacyanoferrate (II) magnetic nano-resins, then at equilibrium, $k_f(C - q_e) - k_b q_e = 0$, because under these conditions:

$$\frac{\partial q}{\partial t} = 0 \text{ or } k_c = \frac{q_e}{(C - q_e)} = \frac{k_f}{k_b} \quad (8)$$

where k_c is the equilibrium constant. Under equilibrium conditions, the rate becomes:

$$\frac{\partial q}{\partial t}[k_f(C - q_t) - k_b q_t] - [k_f(C - q_e) - k_b q_e] \quad (9)$$

If we have,

$$k_f + k_b = \frac{1}{t}\ln\frac{q_e}{q_e - q_t} \quad (10)$$

Therefore,

$$\ln(1 - F_a) = -(k_f + k_b)t = -kt \quad (11)$$

where F_a is the fractional attainment of copper at equilibrium. The kinetic plot of $(1 - F_a)$ vs. t for copper retention on nickel hexacyanoferrate magnetic nano-resins is presented in Fig. 6. The plots exhibit linear relation from which the overall, forward, and backward rate constants were calculated and data are listed in Table 3. The data clarify that forward rate constant was much higher than backward rate constant for removal of copper using both nano-resins. It is pertinent to note that retention of copper was a reversible process and the synthesized nano-resins had a good potential for removal of copper from aqueous solutions. Further, the overall rate constant and forward rate constant for copper removal by WM1 is greater than that for WM2. The equilibrium constant, (k_c) attained the values of 96.58 and 91.38 for WM1 and WM2 nano-resins, respectively.

The sorption kinetic data of Cu(II) retention on magnetic nano-resins were analyzed in term of pseudo-first-order sorption equation. This equation could be written as [38]:

$$\frac{dq_t}{dt} = k_1(q_e - q_t) \quad (12)$$

where q_e and q_t are the amounts of copper retained on nickel hexacyanoferrate (II) magnetic nano-resins at equilibrium and time t (mg g^{-1}), respectively and k_1 is the pseudo-first-order rate constant (min^{-1}). After integration and applying the boundary conditions $q_t = 0$ at $t = 0$ and $q_t = q_t$ at $t = t$, Eq. (12) becomes:

$$\log(q_e - q_t) = \log q_e - \frac{k_1}{2.303}t \quad (13)$$

Table 3
First-order reversible reaction rate constants for removal of copper using nickel hexacyanoferrate magnetic nano-resins.

Rate constant	Resin	
	WM1	WM2
Overall rate constant, (k, min^{-1})	4.1657	3.0568
Equilibrium constant (k_c)	96.58	91.38
Forward rate constant (k_f, min^{-1})	4.123	3.024
Backward rate constant (k_b, min^{-1})	0.0427	0.0331
Correlation coefficient (R^2)	0.974	0.992

When the experimental data were plotted in form of log $(q_e - q_t)$ vs. t, a straight line would be obtained if the pseudo-first-order kinetic model was a suitable expression (Fig. 7). The overleaf of this relation showed approximately linear fit over the entire range of contact time. The values of rate constant (k_1) and equilibrium sorption capacity (q_e) were determined from the slope and intercept of these linear plots and data along with correlation coefficient (R^2) are given in Table 4. The pseudo-first-order rate constant had the values 4.39×10^{-2} and 3.41×10^{-2} min^{-1} for WM1 and WM2 resins, respectively. However, q values estimated from Lagergren plots for Cu(II) retention on WM1 and WM2 nano-resins were 3398, 3590 mg g^{-1}, respectively. These values differed from the experimentally determined q_e values. Therefore, the linearity exhibited by Lagergren plots did not necessarily assure the fitting of pseudo-first-order kinetics in copper retention. This is mainly due to the inherent disadvantage of correctly estimating the equilibrium sorption capacity [39]. Therefore, the pseudo-first-order kinetic model was less likely to explain the rate process.

The deviation detected in fitting pseudo-first-order model had led to further verify the kinetics of Cu(II) retention using pseudo-second-order rate equation that developed by Ho and McKay and expressed as [40,41]:

$$\frac{t}{q_t} = \frac{1}{k_2 q_e^2} + \frac{1}{q_e}t \quad (14)$$

where k_2 is the pseudo-second-order rate constant (g mg^{-1} min^{-1}). The kinetic plots of t/q_t vs. t for copper retention on nickel hexacyanoferrate magnetic nano-resins are presented in Fig. 8. The values of q_e and k_2 were graphically determined from the intercept and slope of revealed plots and summarized in Table 4. They were calculated to be 4901 mg g^{-1} and 3.81×10^{-5} g mg^{-1} min^{-1} for copper retention on WM1 while their values for copper retention on WM2 were 4719 mg g^{-1} and 2.45×10^{-5} g mg^{-1} min^{-1}, respectively. The theoretical q values estimated from pseudo-second-order kinetic

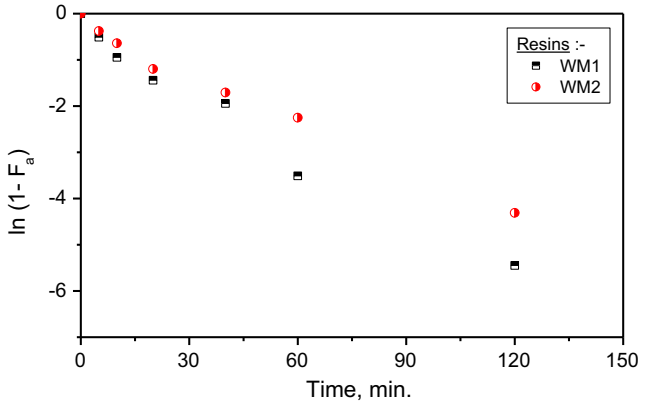

Fig. 6. Reversible first-order kinetic fit for removal of Cu(II) ions using nickel hexacyanoferrate magnetic nano-resins.

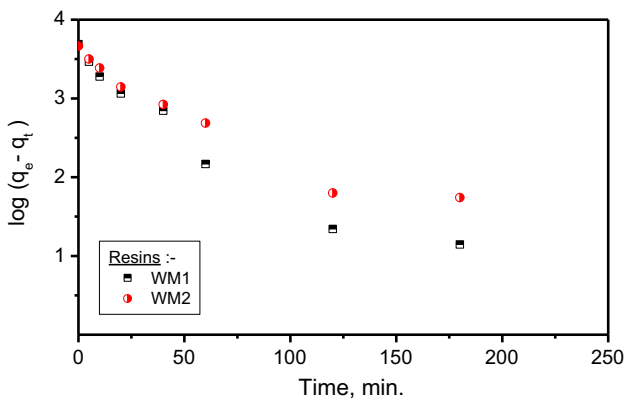

Fig. 7. Lagergren plots for removal of Cu(II) ions using nickel hexacyanoferrate magnetic nano-resins.

Table 4
Kinetic parameters for removal of copper using nickel hexacyanoferrate magnetic nano-resins.

Kinetic model parameters	Resins	
	WM1	WM2
Pseudo first order		
k_1 (min^{-1})	0.0439	0.0341
q_1 (mg g^{-1})	3398	3590
R^2	0.970	0.985
SSE	0.0921	0.0496
Pseudo second order		
k_2 (g mg^{-1} min^{-1})	3.81E-5	2.45E-5
h (mg g^{-1} min^{-1})	952.3	561.8
q_2 (mg g^{-1})	4901	4719
R^2	0.998	0.987
SSE	2.033E-5	1.371E-3

model for both WM1 and WM2 resins agreed with the experimental ones that had the values 4879 and 4690 mg g^{-1}, respectively. This consistence authenticates that the model kinetics fitted well the experimental results for the entire sorption conditions. This confirms that pseudo-second-order sorption kinetics predominate the overall rate of Cu(II) retention that supposed to be controlled by a chemical reaction.

The fitness of applied kinetic models was further assessed by the Squared Sum of Error (SSE) values. It is assumed that the model which gives the lowest SSE values is the best model for metal ion sorption on nickel hexacyanoferrate magnetic nano-resin. The SSE values were calculated using the following equation [9]:

$$SSE = \sum \frac{(q_{t,e} - q_{t,m})^2}{q_{t,e}^2} \quad (15)$$

where $q_{t,e}$ and $q_{t,m}$ are the experimental sorption capacity of copper ions (mg g^{-1}) at time t and the corresponding values obtained from applied kinetic model. SSE values for all kinetic models were calculated and summarized in Table 4. Data clarify that pseudo-second-order model had lower SSE values indicating that retention of Cu(II) on nickel hexacyanoferrate magnetic nano-resins followed pseudo-second-order kinetics.

3.3. Effect of pH

The pH value has been identified as one of the most important parameter that affects the sorption of metal ions. It directly changes the metal ion speciation and their physic-chemical interactions at solid–liquid interface as well as the competition ability of hydrogen ions with these metal ions to the available active sites on resin surface. The effect of initial pH value on removal of Cu(II) by WM1 and WM2 nano-resins were studied at pH range 1–11 and the results are given in Fig. 9. The sorption of Cu(II) onto synthesized nano-resins increased with increasing the initial pH up to 6 and approached a plateau at pH range 6–11. It is worthy to note that sorption of Cu(II) on both WM1 and WM2 was accompanied with a decrease in the final pH values. Such decrease indicates that sorption of Cu(II) resulted in a liberation of proton from the active sites of resins' surface into aqueous solution. At low pH, sorption was low and this may possibly due to the protonation of surface active sites and presence of increased concentration of H_3O^+ ions. Thus, the positively charged surface site and the competition between H_3O^+ and Cu^{2+} ions for the available binding surface site decreased copper uptake in highly acidic medium. With an increase in pH up to 6, the concentration of H_3O^+ ions decreased and the surface active sites became deprotonated and negatively charged, thus the attraction of positively charged Cu^{2+} ions was enhanced. At pH > 6, the removal of Cu^{2+} ions was most likely to onset of copper precipitation as a hydroxide. Similar observations have been early reported for sorption of Cu^{2+} ions on other adsorbents [41].

3.3.1. Speciation

The relationship between the relative amounts of copper ionic species and solution pH was calculated by visual MINTEQ software [42] and presented in Fig. 10. The figure clarifies that copper present in aqueous solution was mainly in Cu^{2+} form up to pH 6. The positively charged $Cu(OH)^+$ appeared in pH range 5–11 while the hydrolytic product $Cu_2(OH)_{;2}^{2+}$ appeared in pH range 6–10. The neutral $Cu(OH)_2$ particles started to precipitate at pH 6.5 and become predominant at pH 9.5. The negatively charged species $Cu(OH)_{;3}^-$ and $Cu(OH)_{;4}^{2-}$ predominated at pH values higher than 11. These evidences argue that electrostatic attraction between Cu^{2+} ions and the positively charged sites in applied nano-resins' surface was unfavorable interaction over the initial pH range 1–6. Further, the complexation equilibria and formation constants of copper hydroxo-complexes are shown below [24]:

$$Cu^{2+} + H_2O \rightleftharpoons CuOH^+ + H^+ \quad \log \beta 1 = -8.22 \quad (16)$$

$$2Cu^{2+} + 2H_2O \rightleftharpoons Cu_2(OH)_{;2}^{2+} + 2H^+ \quad \log \beta 2 = -10.62 \quad (17)$$

It is well recognized that FTIR spectroscopic analysis avouched the presence of a variety of functional groups, such as hydroxyl, cyanide and –Fe–O groups on the surface of prepared magnetic nano-resins. The participation of these functional groups in binding copper ions is highly dependent on pH value of aqueous solutions. This dependence highlights the potential contribution of

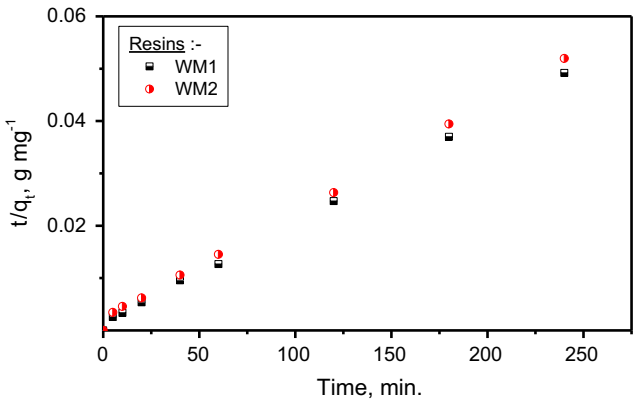

Fig. 8. Pseudo-second-order kinetic fit for removal of Cu(II) ions using nickel hexacyanoferrate magnetic nano-resins.

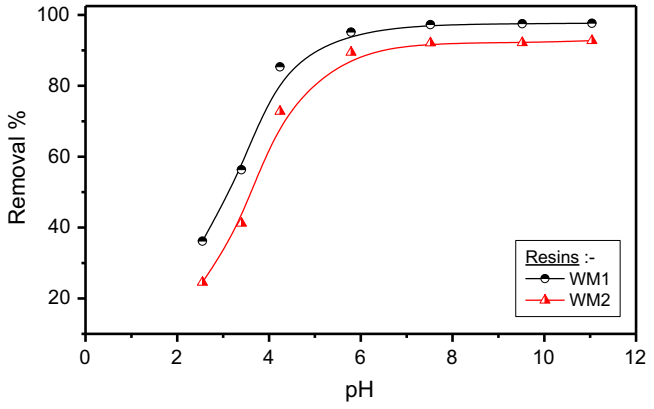

Fig. 9. Effect of solution pH on removal of Cu(II) ions using nickel hexacyanoferrate magnetic nano-resins.

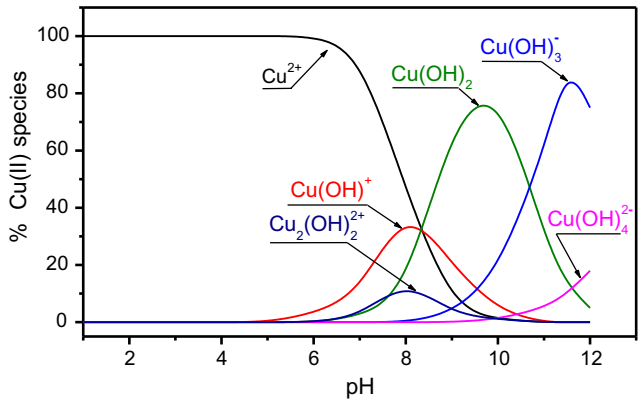

Fig. 10. Speciation diagram of Cu in aqueous solutions at different pH values.

different binding mechanisms in the overall copper retention at different pH values. Depending upon solution pH, iron oxide surface sites can act as a weak acid or base and gain or lose proton (i.e. it can undergo protonation or deprotonation) [43]. Therefore, the following reactions were expected to occur at the surface of prepared magnetic nano-resins in pH range 2–6:

$$-Fe-O^- + H^+ \rightleftharpoons -Fe-OH \quad (18)$$

$$-Fe-OH + H^+ \rightleftharpoons -Fe-OH_2^+ \quad (19)$$

where –Fe–OH represents a single protonated oxide site. The above reactions illustrate that increasing the concentration of deprotonated surface oxide sites could increase the sorption of copper cations that proposed to occur according to the following reaction.

$$-Fe-O^- + Cu^{2+} + H_2O \rightleftharpoons -FeO-Cu(OH) + H^+ \quad (20)$$

In addition, Sun et al. [44] ruled out that zeta potential of these magnetic nano-adsorbents in acidic pH is positive and decreases with increasing pH where the corresponding surface reaction could be expressed as:

$$Fe-OH_2^+ \overset{+H^+}{\leftarrow} Fe-OH \overset{-H^+}{\rightarrow} Fe-O^- \quad (21)$$

Also, hexacyanoferrate is an electroactive anion and its corresponding redox reaction could be written as follows:

$$K_2Ni^{II}[Fe^{II}(CN)_6] \rightleftharpoons KNi^{II}[Fe^{III}(CN)_6] + e^- + K^+ \quad (22)$$

In such a case, a transfer of electron accompanied with simultaneous displacement of potassium ion was revealed [45]. This redox interaction was highly supported by the evidence previously detected by FTIR investigation that confirmed the presence of both hexacyanoferrate (II) and hexacyanoferrate (III) anions.

3.3.2. Retention mechanism and kinetics

The possibility of hexacyanometallates to be used as a reactive resin for copper removal from waste solutions is strongly dependent on their chemical composition and crystal structure as well as the speciation of both analyte cations and surface function groups. In hexacyanometallates, the involved transition metal is usually found with octahedral coordination, crystallizing within the cubic unit cell (Fm–3 m). Further, the alkali metal acts as a charge balancing species within the structure pores and only electrostatic interacted with material frame work. The remaining available space within the cavity is occupied by water molecules, some of them are coordinated to the alkali metal and the others are stabilized within the cavity through hydrogen bonding interactions with the formers.

It is conceivable that metal sorption involves complex participation of different mechanisms as ion exchange, chelation, sorption by physical forces and ion entrapment in inter capillaries and spaces of the structural network. The change in retention mechanism was proposed to be varied with altering solution pH due to the change in the characteristic of reactions that could take place at the solid-solution interface.

In acidic solution, protonation interactions of oxide groups in Fe_3O_4 nanoparticles assure that the protonated oxide groups ($-FeOH_2^+$) are tentatively the dominating surface species that giving rise the surface positive charge density. This surface positivity made copper removal was electrically unfavorable in this region due to the strong electrostatic repulsion. Thus, almost no copper ions were removed at pH < 2. With increasing pH, zeta potential decreased and –Fe–OH became the dominating species around pH 6, the pH_{pzc} value of iron ferrite. At these conditions, retention of Cu^{2+} was hypothesized to be achieved through an ion exchange process according to the following interaction:

$$2Fe-OH + Cu^{2+}(aq) \rightleftharpoons (Fe-O)_2Cu + 2H^+(aq.) \quad (23)$$

Such proton liberation from –Fe–OH groups into aqueous solution clearly elucidates the decrease in final pH values that accompanied with copper retention progress. In addition, a release of K^+ ions was proposed to occur from potassium nickel hexacyanoferrate (II) structure to aqueous solution. This release might be resulted from the redox interactions of $Fe^{(II,III)}{}_3O_4@K_2Ni[Fe^{(II,III)}(CN)_6]$ magnetic nano-resin. In such a case, retention of copper could be predicted to be attained through an exchange of K^+ ions with Cu^{2+} cations yielding $CuNi[Fe(CN)_6]$. Thus, the significant removal of copper ions occurred at pH range 2–6 was suggested to be attained through molar exchange of single Cu^{2+} ions with K^+ and/or H^+ ions.

The retention mechanism was predicted to be quite different in neutral solutions where copper presents in different three cationic species are Cu^{2+}, $Cu(OH)^+$ and $Cu_2(OH)_2^{2+}$ besides $Cu(OH)_2$. These species were supposed to be retained at the magnetic nano-resin surface either by ion exchange mechanism or by hydrogen bonding as shown below:

$$-R-OH + CuOH^+ \rightarrow -RO-CuOH + H^+ \quad \text{(Ion exchange)} \quad (24)$$

$$2(-R-OH) + Cu_2(OH)_2^{2+} \rightarrow -(RO)_2-Cu(OH)_2 + 2H^+ \quad \text{(Ion exchange)} \quad (25)$$

$$2(-R-OH) + Cu(OH)_2 \rightarrow (-ROH)_2-Cu(OH)_2 \quad \text{(H-bonding)} \quad (26)$$

where –R represents the matrix of resin phase. Besides, copper that has an incomplete octet of electrons can act as a Lewis acid and interacts with –CN group in hexacyanoferrate structure that acts a Lewis base, and produces a coordinated complex. Under these conditions, surface complexation interactions were expected to participate in the overall retention of copper at this pH range. It is conceivable that all previously mentioned mechanisms work together and play a critical role in the overall removal of Cu(II) although it is difficult to quantitatively estimate the extent of removal referred to any of them. At higher pH values, the strong decrease in aqueous copper concentration shows that precipitation was a relevant mechanism taking place in Cu(II) retention besides the possibly simultaneous contributions of other mechanisms over pH range 6–11.

The removal of copper ions attained through different sorption mechanisms could be limited by the kinetics of their accessibility to the inter–planar space of Fm–3 m crystal structure. These kinetics were explored with the theory proposed by Weber and Morris

for intraparticle diffusion [46]. They clarified that intraparticle diffusion is often regarded as the rate-limiting step in most sorption processes and stated that the sorbed amount (q_t) almost varies with the square root of contact time ($t^{0.5}$). The linear form of intraparticle diffusion equation is give as:

$$q_t = k_{\text{int}} t^{0.5} \tag{27}$$

where q_t is the amount adsorbed at time t (mg g^{-1}), t is the time (min), and k_{int} is the intraparticle diffusion rate constant (mg g^{-1} min$^{-0.5}$). If intraparticle diffusion is the sole mechanism taking place, a plot of sorption capacity q_t at time t vs. $t^{0.5}$ would yield a straight line. The overleaf shows two regions with two linear segments had different slops. The initial segments were attributed to the diffusion of copper ions from bulk solution to nano-resin surface. The second segments describe the gradual retention to attain equilibrium stage and represents the diffusion of copper ions within the resin structure. It is pertinent to note that the linear diffusion plots did not pass through the origin, and hence intraparticle diffusion may not be the sole factor controlling the mechanism of copper retention (see Supplementary data). The value of k_{int} was calculated from the slope of straight lines and given in Table 5. k_{int} had the values 0.0949 and 0.1191 mg g^{-1}min$^{-0.5}$ for WM1 and WM2 resins, respectively. These results authenticate that a large number of Cu(II) ions might have diffused into the pores before being adsorbed.

3.4. Sorption isotherm

Sorption isotherms are mathematical models that describe the distribution of adsorbate species among liquid and adsorbent phases, based on a set of assumptions. Analysis of isotherm data is important for predicting the sorption capacity of adsorbent, which is one of the main parameters required for design of a sorption system. Several isotherm models were used for this purpose. To find out the mechanistic parameters associated with Cu(II) sorption, the results obtained were analyzed using the well-known models given by Freundlich and Langmuir.

Freundlich isotherm is the earliest known relationship, which assumes that the surface sites of an adsorbent have different binding energies. Freundlich expression is an empirical equation describes sorption occurring onto heterogeneous surfaces and addresses reversible sorption process not restricted to monolayer formation. This model provides no information on the monolayer sorption capacity and considers that sorption takes place in multi-sites due to the heterogeneity on the surfaces. The basic assumption of Freundlich isotherm is that if the concentration of a solute in a solution at equilibrium, C_e, was raised to the power $1/n$, then $C_e^{1/n} q_e$ was a constant at a given temperature. The non-linear form of Freundlich equation is given as follows [47]:

$$q_e = k_F C_e^{1/n} \tag{28}$$

where k_F is Freundlich constant (mg g^{-1}), and n is an empirical constant indicates the sorption intensity. The value of n indicates a favorable sorption for the range $1 < n < 10$. Taking log and rearranging Eq. (28), the linear form of Freundlich equation is expressed as:

$$\log q_e = \log k_F + \frac{1}{n} \log C_e \tag{29}$$

The values of k_F and n constants were determined directly from the intercept and slope of the straight lines revealed by plotting log q_e vs. log C_e. The data were extrapolated using the least-squared linear regression to calculate k_F and n and the values are given in Table 6. Freundlich isotherm constant (k_F) had the values 6740 and 1812 mg g^{-1} for Cu(II) sorption on WM1 and WM2 while the corresponding n values were 2.12 and 1.26, respectively.

Langmuir isotherm model describes monolayer coverage of an adsorbate on a homogeneous adsorbent surface through a chemisorption process. It assumes sorption to take place only at specific site on adsorbent surface. Moreover, all active sites are also assumed to be energetically equivalent and distant to each other and there is no interaction between species adsorbed on adjacent active sites. The model is characterized by linear sorption at low surface coverage, which becomes non-linear as sorption sites approach saturation. In addition, sorption energies and enthalpies are uniform for each site. Langmuir model equation is illustrated as [40]:

$$q_e = \frac{q_m k_L C_e}{1 + k_L C_e} \tag{30}$$

where q_e is the amount of Cu(II) adsorbed per unit weight of nano-resin (mg g^{-1}) at equilibrium, C_e is the equilibrium concentration of Cu(II) ions in solution (mg L^{-1}), q_m is the maximum sorption capacity of synthesized nano-resins (mg g^{-1}), k_L is Langmuir affinity constant (L mg^{-1}). The linearized form of Langmuir model is given as:

$$\frac{1}{q_e} = \frac{1}{q_m k_L}\left(\frac{1}{C_e}\right) + \frac{1}{q_m} \tag{31}$$

The values of q_m and k_L were graphically determined from the intercept and slope of the linear plot of $1/q$ vs. $1/C$. The data had been extrapolated using the least-squared linear regression to calculate the model constants and the values are tabulated in Table 6. Data indicate that WM1 exhibited high retention ability for Cu(II) compared with that of WM2 and attained a calculated sorption capacity of 4777 mg g^{-1} compared with 4336 mg g^{-1} for WM2. The values of k_L were found to be 0.316 and 1.67 L mg^{-1} for WM1 and WM2, respectively.

The affinity of potassium nickel hexacyanoferrate magnetic nano-resins for Cu(II) retention was further predicted using Langmuir dimensionless separation factor R_L that is given by the relation:

$$R_L = \frac{1}{1 + k_L C_0} \tag{32}$$

where C_0 is the initial Cu(II) concentration (mg L^{-1}). R_L values within the range $0 < R_L < 1$ indicate favorable sorption. The values of R_L were determined and tabulated in Table 6. In this study, all R_L values were fallen within 0 and 1 and this indicated a highly favorable sorption with increasing sorption efficiency at higher Cu(II) concentrations.

An error function was also employed to compare the obtained experimental data with that predicted from the applied isotherm models. The Chi-squared test (χ^2) correlates the sum of the squares of the differences between experimental data and model predictions, with each squared difference divided by the corresponding model prediction. The nonlinear Chi-square test (χ^2) and the linear correlation coefficients (R^2) are represented mathematically as [13]:

$$\chi^2 = \sum \frac{(q_e - q_{e,m})^2}{q_{e,m}} \tag{33}$$

Table 5
Intraparticle diffusion kinetic constants for removal of copper using nickel hexacyanoferrate magnetic nano-resins.

Sample	k_{int} (mg g^{-1} min$^{-0.5}$)		Intercept		R^2
	Value	SE[a]	Value	SE	
WM1	0.0949	0.030	3.616	0.316	0.641
WM2	0.1191	0.026	2.987	0.277	0.794

[a] Standard Errors.

Table 6
Isotherm models' constants for removal of copper using nickel hexacyanoferrate magnetic nano-resins.

Resins	Freundlich model				Langmuir model				
	k_F (mg g^{-1})	n	R^2	χ^2	q_m (mg g^{-1})	k_L (L mg^{-1})	R_L	R^2	χ^2
WM1	6740	2.12	0.977	0.55	4777	3.16E-1	5.96E-2	0.968	1.37
WM2	1812	1.26	0.976	6.83	4336	1.67	1.18E-2	0.945	11.26

$$R^2 = \frac{\sum(q_{e,m} - \bar{q}_e)^2}{\sum(q_{e,m} - \bar{q}_e)^2 + \sum(q_{e,m} - q_e)^2} \quad (34)$$

where q_e is the experimental value of equilibrium sorption capacity (mg g^{-1}), $q_{e,m}$ is the value calculated from model equation (mg g^{-1}), and $\bar{q}_e$ is the average of q_e values. It should be noted that if a model prediction is similar to the experimental data, χ^2 will approach zero, and if they differ from each other, χ^2 will have a big number. Therefore, it is necessary to analyze the data using the non-linear Chi-square test to confirm the isotherm that best fits the studied sorption system. The modeled values of correlation coefficients (R^2) and non-linear Chi-square test (χ^2) for both isotherm models are shown in Table 6. Freundlich isotherm model appeared to best fit the sorption of Cu(II) onto WM1 and WM2 resins where it exhibited the highest correlation coefficient and lowest Chi-square values. The model had R^2 and Chi-square values amounted to 0.977 and 0.55 for copper sorption onto WM1 beads and 0.976 and 6.83 values for sorption onto WM2 beads. Contrarily, Langmuir isotherm model had lowest correlation coefficients (R^2) and high Chi-square (χ^2) values for copper sorption onto both nano-resins. This indicates that sorption of Cu(II) onto the synthesized nano-resins is not homogeneous process.

The non-linear fit of Freundlich and Langmuir isotherm models to the experimental results of copper retention onto both WM1 and WM2 magnetic nano-resins is presented in Fig. 11. The plots demonstrate that Freundlich model is more appropriate to describe the removal of Cu(II) using nickel hexacyanoferrate magnetic nano-resins along with applied concentration range. Contrary, the non-linear fit of Langmuir isotherm model only concordat experimental results at low initial concentrations, while at higher initial concentrations it deviates from experimentally determined q values. The avouched deviation argued the improbability of Langmuir isotherm model to fit the studied system under applied conditions. This discordance could be considered a reason for the odd behavior revealed with Langmuir non-linear fit for WM1 and WM2 samples. Further, this observation coincides well with correlation coefficients (R^2) and Chi-square (χ^2) values previously determined. Accordingly, copper ions were supposed to be retained on heterogeneous surface through reversible non-linear process forming multi-linear formations.

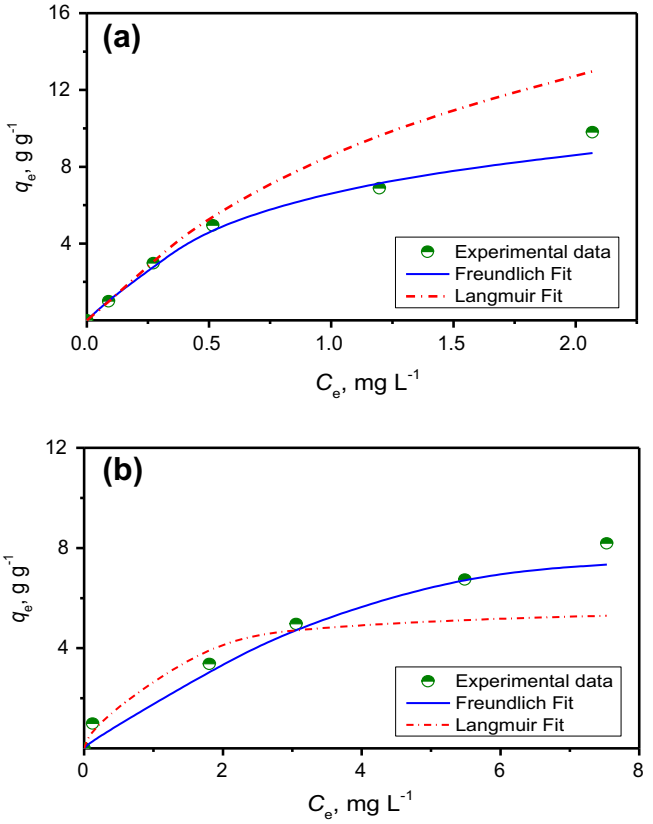

Fig. 11. Non-linear isotherm models of Langmuir and Freundlich for removal of Cu(II) ions using magnetic nano-resins: (a) WM1 and (b) WM2.

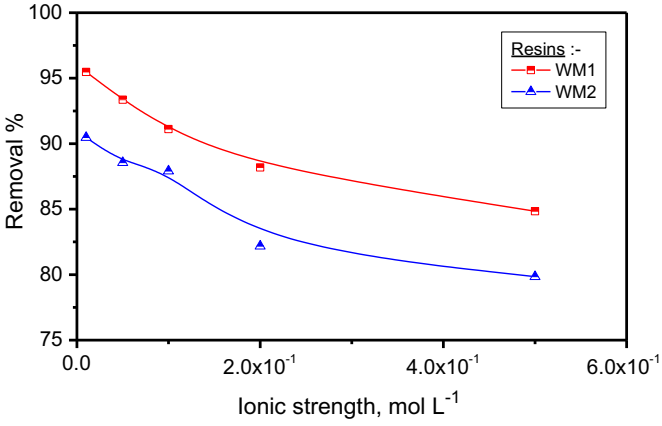

Fig. 12. Effect of background electrolyte on removal of Cu(II) ions using nickel hexacyanoferrate magnetic nano-resins.

3.5. Ionic strength

The role of ionic strength of aqueous solution on sorption of Cu(II)) was investigated using NaCl as a background electrolyte. The solution ionic strength was set to have a range from 0.01 to 0.5 mol L^{-1} and the revealed data are depicted in Fig. 12. The results clarify that sorption process was ionic strength-dependent where the sorption extent decreased from 96.4% to 84% for Cu(II) sorption onto WM1 and from 90% to for 79% for sorption onto WM2 in coexistence of 0.5 M NaCl as a background electrolyte.

In aqueous solutions, cupper ions can act as a Lewis acid and interact with an electron-pair donating surface function groups (such as: cyanide (–CN) which acts as a Lewis basis in its deprotonated form and forms a Lewis salt-type compound. In such a case, water molecules would be interposed between the surface functional group and Cu^{2+} ions and a surface complex of type "outer-sphere complex" would be formed as:

$$-CN + Cu(OH_2)_{;n}^{2+} \rightleftharpoons -CN(H_2O)Cu + (n-1)H_2O \quad (35)$$

It well recognized that, copper retention onto nickel hexacyanoferrate magnetic nano-resin depends on the speciation of this cation and its mode of interaction with the active sites in nano-resin surface. In chloride medium, uncharged species (e.g. $CuCl_2$) and charged complexes (e.g. $CuCl^+$, $CuCl_3^-$ etc.) were supposed to be formed. These chloro-species are less strongly adsorbed because they have lower affinities to resin surface compared with that of Cu^{2+} ions. Further, they did not form tertiary complexes. Hence, the co-existence of Cl^- ions limited the sorption of copper from aqueous solutions containing NaCl electrolyte. Also, Na^+ ions could compete with Cu^{2+} ions for the available sites in resin surface and hence negatively affected the removal efficiency. These findings are coincident with previously reported results [48]. Other authors reported that the reduction in percentage of metal removal was attributed to the differences in modes of particle association such as: (a) edge-to-edge (EE); (b) edge-to-face (EF); and (c) face-to-face (FF) [49]. They clarified that as the concentration of background electrolyte increases, it is likely that particle association changes from EE to EF mode, thus blocking and reducing the amount of faces available for Cu(II) sorption.

4. Conclusion

In this study, a procedure for synthesis of a novel magnetic nano-resin was established. The procedure was based deposition of insoluble nickel hexacyanoferrates on magnetic nano-particles of Fe_3O_4 and immobilizing them within a polymeric matrix. The synthesized magnetic nano-resins showed satisfactory characteristics to effectively remove copper ions from aqueous solutions. They exhibited good exchange kinetics and high sorption capacity. Copper retention was a sensitive process directly dependent on pH value and indirectly dependent on ionic strength of aqueous solutions. Further, the sorption mechanism was strongly dependent on the speciation of both function groups on resins' surface and copper ions at solid-liquid interface. Ion exchange played a significant role in the overall removal of Cu(II) besides the participation, to some extent, of other mechanisms as complexation interactions and precipitation. The results argue that Cu(II) retention followed pseudo-second-order kinetics and controlled by chemical reaction. It well recognized that copper was retained on a heterogeneous surface forming multi-linear formations through a reversible non-linear process. Finally, the study authenticates that the synthesized magnetic nano-resin could be considered as a quiet and efficient adsorbent for fast removal of heavy metals from aqueous solutions.

Appendix A. Supplementary material

Supplementary data associated with this article can be found, in the online version, at http://dx.doi.org/10.1016/j.cej.2012.09.113.

References

[1] X.J. Ju, S.B. Zhang, M.Y. Zhou, R. Xie, J. Yang, L.Y. Chu, Novel heavy-metal adsorption material: ion-recognition P(NIPAM-co-BCAm) hydrogels for removal of lead(II) ions, J. Hazard. Mater. 167 (2009) 114–118.

[2] J.I. Simionato, A.T. Paulino, J.C. Garcia, J. Nozaki, Adsorption of aluminum from wastewater by chitin and chitosan produced from silkworm chrysalides, Polym. Int. 55 (2006) 1243–1248.

[3] R.R. Sheha, H.H. Someda, Hazardous Wastes: Classification and Treatment Technologies, Nova Science Publishers, Inc., New York, 2008.

[4] T.G. Kazi, N. Jalbani, N. Kazi, M.B. Arain, M.K. Jamali, H.I. Afridi, G.A. Kandhro, R.A. Sarfraz, A.Q. Shah, R. Ansari, Estimation of toxic metals in scalp hair samples of chronic kidney patients, Biol. Trace Elem. Res. 127 (2009) 16–27.

[5] H.I. Afridi, T.G. Kazi, N.G. Kazi, M.B. Arain, N. Jalbani, R.A. Sarfraz, A.Q. Shah, J.A. Baig, Evaluation of arsenic, cobalt, copper and manganese in biological samples of steel mill workers by electrothermal atomic absorption spectrometry, Toxicol. Ind. Health 25 (2009) 59–69.

[6] M.B. Arain, T.G. Kazi, M.K. Jamali, N. Jalbani, H.I. Afridi, A. Shah, Total dissolved and bioavailable elements in water and sediment samples and their accumulation Oreochromis mossambicus of polluted Manchar Lake, Chemosphere 70 (2008) 1845–1856.

[7] Y.H. Huang, C.L. Hsueh, H.P. Cheng, L.C. Su, C.Y. Chen, Thermodynamics and kinetics of adsorption of Cu(II) onto waste iron oxide, J. Hazard. Mater. 144 (2007) 406–411.

[8] H. Aydin, Y. Bulut, C. Yerlikaya, Removal of copper (II) from aqueous solution by adsorption onto low-cost adsorbents, J. Environ. Manage. 87 (2008) 37–45.

[9] V.S. Munagapati, V. Yarramuthi, S.K. Nadavala, S.R. Alla, K. Abburi, Biosorption of Cu(II), Cd(II) and Pb(II) by Acacia leucocephala bark powder: kinetics, equilibrium and thermodynamics, Chem. Eng. J. 157 (2010) 357–365.

[10] S.S. Hindo, A.M. Mancino, J.J. Braymer, Y. Liu, S. Vivekanandan, A. Ramamoorthy, M.H. Lim, Small molecule modulators of copper-induced Aβ aggregation, J. Am. Chem. Soc. 131 (2009) 16663–16665.

[11] S.S. Banerjee, D.H. Chen, Fast removal of copper ions by gum Arabic modified magnetic nano-adsorbent, J. Hazard. Mater. 147 (2007) 792–799.

[12] Y. Ren, X. Wei, M. Zhang, Adsorption character for removal Cu(II) by magnetic Cu(II) ion imprinted composite adsorbent, J. Hazard. Mater. 158 (2008) 14–22.

[13] A.T. Paulino, L.A. Belfiore, L.T. Kubota, E.C. Muniz, V.C. Almeida, E.B. Tambourgi, Effect of magnetite on the adsorption behavior of Pb(II), Cd(II), and Cu(II) in chitosan-based hydrogels, Desalination 275 (2011) 187–196.

[14] A. Ngomsik, A. Bee, M. Draye, G. Cote, V. Cabuil, Magnetic nano and microparticles for metal removal and environmental applications: a review, C. R. Chimie. 8 (2005) 963–970.

[15] Y.F. Shen, J. Tang, Z.H. Nie, Y.D. Wang, Y. Ren, L. Zuo, Preparation and application of magnetic Fe_3O_4 nanoparticles for wastewater purification, Sep. Purif. Technol. 68 (2009) 312–319.

[16] R.R. Sheha, A.A. El-Zahhar, Application of magnetic materials in separation technologies, in: Jacob.I. Levine (Ed.), Magnetic Materials: Research, Technology and Applications, Nova Science Publishers, Inc., New York, 2009.

[17] O. Ozay, E. Ekici, Y. Baran, N. Aktas, N. Sahiner, Removal of toxic metal ions with magnetic hydrogels, Water Res. 43 (2009) 4403–4411.

[18] Y.C. Chang, S.W. Chang, D.H. Chen, Magnetic chitosan nanoparticles: studies on chitosan binding and adsorption of Co(II) ions, React. Funct. Polym. 66 (2006) 335–341.

[19] A.Z. Maor, R. Semiat, H. Shemer, Synthesis, performance, and modeling of immobilized nano-sized magnetite layer for phosphate removal, J. Colloid Interface Sci. 357 (2011) 440–446.

[20] R.R. Sheha, A.A. El-Zahhar, Synthesis of some ferromagnetic composite resins and their metal removal characteristics in aqueous solutions, J. Hazard. Mater. 150 (2008) 795–805.

[21] J. Hu, M.C. Lo-Irene, G.H. Chen, Performance and mechanism of chromate (VI) adsorption by –FeOOH-coated maghemite (–Fe_2O_3) nanoparticles, Sep. Purif. Technol. 58 (2007) 76–82.

[22] Y.C. Chang, D.H. Chen, Preparation and adsorption properties of monodisperse chitosan-bound Fe_3O_4 magnetic nanoparticles for removal of Cu(II) ions, J. Colloid Interface Sci. 283 (2005) 446–451.

[23] J. Hizal, R. Apak, Modeling of cupper(II) and lead(II) adsorption on kaolinite-based clay minerals individually and in the presence of humic acid, J. Colloid Interface Sci. 295 (2006) 1–13.

[24] Y. Wang, S. Huang, S. Kang, C. Zhang, X. Li, Low-cost route for synthesis of mesoporous silica materials with high silanol groups and their application for Cu(II) removal, Mater. Chem. Phys. 132 (2012) 1053–1059.

[25] R.D. Ambashta, P.K. Wattal, S. Singh, D. Bahadur, Nano-aggregates of hexacyanoferrate (II)-loaded magnetite for removal of cesium from radioactive wastes, J. Magn. Magn. Mater. 267 (2003) 335–340.

[26] W.Q. Cai, J.G. Yu, M. Jaroniec, Template-free synthesis of hierarchical spindlelike γ-Al_2O_3 materials and their adsorption affinity towards organic and inorganic pollutants in water, J. Mater. Chem. 20 (2010) 4587–4594.

[27] J. Zhou, S. Yang, J. Yu, Facile fabrication of mesoporous MgO microspheres and their enhanced adsorption performance for phosphate from aqueous solutions, Colloids Surf. Physicochem. Eng. Aspects 379 (2011) 102–108.

[28] Q. Lan, L. Chao, F. Yang, S.Y. Liu, J. Xu, D.J. Sun, Synthesis of bilayer oleic acid coated Fe_3O_4 nanoparticles and their application in pH-responsive pickering emulsions, J. Colloid Interface Sci. 310 (2007) 260–269.

[29] Y.K. Leong, U. Seah, S.Y. Chu, B.C. Ong, Effect of gum arabic macromolecules on surface forces in oxide dispersion, Colloid Surf. 182 (2001) 263–268.

[30] M.J. Holgado, V. Rives, M.S. Sanromain, P. Malet, Solid State Ionics 92 (1996) 273.

[31] J.T. Rajamathi, N.H. Raviraj, M.F. Ahmed, M. Rajamathi, Hexacyanoferrate-intercalated nickel zinc hydroxy double salts, Solid State Sci. 11 (2009) 2080–2085.

[32] C. Loos-Neskovic, S. Ayrault, V. Badillo, B. Jimenez, E. Garnier, M. Fedoroff, D.J. Jones, B. Merinov, Structure of copper–potassium hexacyanoferrate (II) and sorption mechanisms of cesium, J. Solid State Chem. 177 (2004) 1817–1828.

[33] M. Mostafa, M.A. El-Absy, M. Amin, M.A. El-Amir, A.B. Farag, Partial purification of neutron-activation ^{99}Mo from cross-contaminant radionuclides onto potassium nickel hexacyanoferrate(II) column, J. Radioanal. Nucl. Chem. 285 (2010) 579–588.

[34] Y.M. Al-Angari, Magnetic properties of La-substituted $NiFe_2O_4$ via egg-white precursor route, J. Magn. Magn. Mater. 323 (2011) 1835–1839.

[35] D. Cullity, Elements of X-ray Diffraction, second ed., Addison-Wesley, London, 1978.

[36] M. Ismail, M.R. El-Sourougy, N. Abdel Moneim, H.F. Aly, Preparation, characterization, and utilization of potassium nickel hexacyanoferrate for the separation of cesium and cobalt from contaminated waste water, J. Radioanal. Nucl. Chem. 237 (1998) 97–103.
[37] S. Rengaraj, Y. Kim, C.K. Joo, K. Choi, J. Yi, Batch adsorptive removal of copper ions in aqueous solutions by ion exchange resins: 1200H and IRN97H, Korean J. Chem. Eng. 21 (1) (2004) 187–194.
[38] S.A. Ahmed, Batch and fixed-bed column techniques for removal of Cu(II) and Fe(III) using carbohydrate natural polymer modified complexing agents, Carbohyd. Polym. 83 (2011) 1470–1478.
[39] Y.S. Ho, G. McKay, The sorption of lead(II) ions on peat, Water Res. 33 (1999) 578–584.
[40] Y.S. Ho, G. McKay, Kinetic models for the sorption of dye from aqueous solution by wood, Trans. Inst. Chem. Eng. 76B (1998) 183–191.
[41] K.G. Bhattacharyya, S.S. Gupta, Removal of Cu(II) by natural and acid-activated clays: An insight of adsorption isotherm, kinetic and thermodynamics, Desalination 272 (2011) 66–75.
[42] J.P. Gustafsson, <www.lwr.kth.se/English/OurSoftware/vminteq/verhistory.htm>, 2009.
[43] S.S. Banerjee, R.V. Jayaram, M.V. Joshi, Removal of Cr(VI) and Hg(II) from aqueous solutions using fly ash and impregnated fly ash, Sep. Sci. Technol. 39 (2004) 1611–1629.
[44] Z.X. Sun, F.W. Su, W. Forsling, P.O. Samskog, Surface characteristics of magnetite in aqueous suspension, J. Colloid Interface Sci. 197 (1998) 151–159.
[45] A. Abbaspour, A. Khajehzadeh, A. Ghaffarinejad, Electrocatalytic oxidation and determination of hydrazine on nickel hexacyanoferrate nanoparticles-modified carbon ceramic electrode, J. Electroanal. Chem. 631 (2009) 52–57.
[46] J.R. Weber, J.C. Morris, Kinetics of adsorption on carbon from solution, J. Sanit. Eng. Div. Am. Soc. Eng. 89 (1963) 31–39.
[47] Q. Li, J. Zhai, W. Zhang, M. Wang, J. Zhou, Kinetic studies of adsorption of Pb(II), Cr(III) and Cu(II) from aqueous solution by sawdust and modified peanut husk, J. Hazard. Mater. 141 (2007) 163–167.
[48] S. Lee, J. Yang, Removal of copper in aqueous solutions by apple wastes, Sep. Sci. Technol. 32 (1997) 1371–1387.
[49] D.E. Egirani, A.R. Baker, J.E. Andrews, Copper and zinc removal from aqueous solution by mixed mineral systems II. The role of solution composition and aging, J. Colloid Interface Sci. 291 (2005) 326–333.